JACS
JOURNAL OF THE AMERICAN CHEMICAL SOCIETY

Article

pubs.acs.org/JACS

Atomic Structure of Pt_3Ni Nanoframe Electrocatalysts by *in Situ* X-ray Absorption Spectroscopy

Nigel Becknell,[†] Yijin Kang,[‡] Chen Chen,[†,▽] Joaquin Resasco,[§] Nikolay Kornienko,[†] Jinghua Guo,[∥] Nenad M. Markovic,[‡] Gabor A. Somorjai,[†,⊥] Vojislav R. Stamenkovic,[‡] and Peidong Yang*[,†,⊥,#]

[†]Department of Chemistry, University of California, Berkeley, California 94720, United States
[‡]Materials Science Division, Argonne National Laboratory, Argonne, Illinois 60439, United States
[§]Department of Chemical Engineering, University of California, Berkeley, California 94720, United States
[∥]The Advanced Light Source, Lawrence Berkeley National Laboratory, Berkeley, California 94720, United States
[⊥]Materials Sciences Division, Lawrence Berkeley National Laboratory, Berkeley, California 94720, United States
[#]Kavli Energy Nanoscience Institute, Berkeley, California 94720, United States

Supporting Information

ABSTRACT: Understanding the atomic structure of a catalyst is crucial to exposing the source of its performance characteristics. It is highly unlikely that a catalyst remains the same under reaction conditions when compared to as-synthesized. Hence, the ideal experiment to study the catalyst structure should be performed *in situ*. Here, we use X-ray absorption spectroscopy (XAS) as an *in situ* technique to study Pt_3Ni nanoframe particles which have been proven to be an excellent electrocatalyst for the oxygen reduction reaction (ORR). The surface characteristics of the nanoframes were probed through electrochemical hydrogen underpotential deposition and carbon monoxide electrooxidation, which showed that nanoframe surfaces with different structure exhibit varying levels of binding strength to adsorbate molecules. It is well-known that Pt-skin formation on Pt−Ni catalysts will enhance ORR activity by weakening the binding energy between the surface and adsorbates. *Ex situ* and *in situ* XAS results reveal that nanoframes which bind adsorbates more strongly have a rougher Pt surface caused by insufficient segregation of Pt to the surface and consequent Ni dissolution. In contrast, nanoframes which exhibit extremely high ORR activity simultaneously demonstrate more significant segregation of Pt over Ni-rich subsurface layers, allowing better formation of the critical Pt-skin. This work demonstrates that the high ORR activity of the Pt_3Ni hollow nanoframes depends on successful formation of the Pt-skin surface structure.

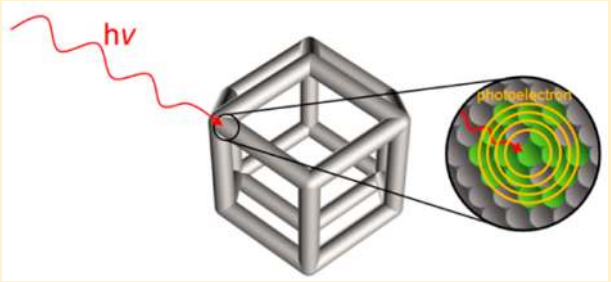

INTRODUCTION

The world's growing energy demand and finite fossil fuel resources combined with the documented anthropogenic effect on the climate has motivated a significant growth in research on renewable energy technologies.[1,2] One current area of emphasis is materials and systems for electrocatalytic and photoelectrochemical water splitting to produce hydrogen as an energy carrier.[3] To efficiently use this hydrogen, performance of proton exchange membrane fuel cells (PEMFC) must be improved. The limitation for commercialization of the PEMFC is currently the design of an efficient, cheap, and stable catalyst for the bottleneck cathodic oxygen reduction reaction (ORR). It is well known that platinum is the top performing monometallic catalyst for the ORR in acidic electrolytes.[4,5] However, the cost of platinum, a rare element, has proven to be a limiting factor in the large-scale production and commercialization of fuel cells in transportation.[6] The goal in catalyst design has therefore been to reduce the quantity of platinum required for a fuel cell by increasing activity while minimizing the fraction of platinum in the ORR catalyst.[7]

A major breakthrough was made in the discovery that the formation of Pt-skin—a single atomic layer of platinum—over the surface of a $Pt_3Ni(111)$ single crystal through high-temperature annealing led to an order-of-magnitude increase in specific activity over the Pt(111) single crystal surface.[8] The significant increase in activity was attributed to the alteration of the surface electronic density of states due to the segregation of platinum to the surface and nickel to the subsurface layer. This results in a lower center of gravity for the surface *d*-band states with respect to the Fermi level, which weakens the binding energy between adsorbates and the Pt-skin surface.[9−11] This can be identified by electrochemical surface area (ECSA) estimation via underpotentially deposited hydrogen (H_{upd}) and carbon monoxide electrooxidation (CO_{ad}).[12−14] On a Pt-skin surface, underpotentially deposited hydrogen exhibits lower surface coverage due to weakened binding, which leads to underestimation of the ECSA. However, the ECSA obtained

Received: September 14, 2015
Published: December 10, 2015

DOI: 10.1021/jacs.5b09639
J. Am. Chem. Soc. 2015, 137, 15817−15824

from electrooxidation of CO_{ad} experiments, or CO-stripping, remains unaffected. This phenomenon yields a characteristic value of the ratio between ECSA determined from CO_{ad} and H_{upd} (CO_{ad}:H_{upd}) of approximately 1.5. This has proven to be an easy way to identify formation of the Pt-skin surface structure over Pt_3Ni electrocatalysts.

Many attempts have been made to replicate the surface conditions of the $Pt_3Ni(111)$-skin at the nanoscale in order to utilize the high specific activity of the Pt-skin surface and obtain nanocatalysts with uniquely high mass activity.[15−24] We recently reported a novel architecture of highly active nanostructure, termed nanoframe, which was synthesized by first making a $PtNi_3$ rhombic dodecahedron with platinum enriched edges of its three-dimensional shape.[25] This distinct, non-uniform distribution of platinum allowed for the faces and interior of the rhombic dodecahedron to be eroded away by solution-phase spontaneous oxidation and corrosion of nickel, eventually converting the structure to a hollow Pt_3Ni nanoframe. After annealing, electrochemical measurements of the CO_{ad}:H_{upd} ratio yielded a value of ∼1.5, confirming that heat treatment could induce the formation of the desired Pt-skin on this nanostructure. The nanoframe electrocatalyst with Pt-skin demonstrated extremely high activity with 36 times increase in mass activity and 22 times in specific activity over Pt/C catalysts.

In order to gain atomic insight into structural factors which contribute to trends in catalytic activity, materials of interest must be studied under reaction conditions (*in situ*). It is generally accepted that a catalyst characterized *ex situ* will not necessarily maintain the same properties under reaction conditions, and for that reason, these systems have been studied *in situ* by techniques such as sum frequency generation,[26] X-ray photoelectron spectroscopy,[27] and X-ray absorption spectroscopy (XAS).[28] XAS is an ideal technique for *in situ* studies because it is minimally invasive and the X-rays can penetrate through thin walls typically made of silicon nitride or carbon-based materials in specially designed reactors.[29] The technique can be used to gain information about oxidation states, electronic structure, and chemical ordering of materials among other properties. Recently, XAS has been widely used to study ORR catalysts *in situ* to illustrate the dependence of their catalytic activity on ordering of an alloy,[30] Pt shell thickness,[31] and Pt−Pt bond lengths[32] and to study oxide formation at the Pt-electrolyte interface.[33,34] Here, we have used *ex situ* and, critically, *in situ* X-ray absorption spectroscopy techniques to lend more understanding to the nature and success of Pt-skin formation on Pt_3Ni nanoframes which have proven to be one of the best known ORR nanocatalysts to date.

EXPERIMENTAL SECTION

Synthesis of $PtNi_3$ Nanopolyhedra. Twenty milligrams of $H_2PtCl_6{\cdot}6H_2O$ and 17.5 mg of $Ni(NO_3)_2{\cdot}6H_2O$ were dissolved in 0.4 mL of deionized water, forming a transparent yellow solution. Ten milliliters of oleylamine was preheated in a three-necked flask at 160 °C for 1 h with argon purging, after which the aqueous precursor solution was injected. The reaction was held at 160 °C for 3 min under vacuum to remove water. The reaction system was further heated to 265 °C under argon atmosphere. After reaching 265 °C, the solution turned from transparent to black. After it had turned black, the reaction solution was then held for a further 3 min for growth of the particles. The reaction was stopped by rapidly cooling the solution down to room temperature. The synthesized $PtNi_3$ nanopolyhedra were washed once by ethanol and a second time by hexane and ethanol and were collected by centrifugation (8000 rpm) after each wash. The washed product was re-dispersed in either hexanes or chloroform.

Evolution from $PtNi_3$ Nanopolyhedra to Pt_3Ni Nanoframes. The $PtNi_3$ nanopolyhedra were re-dispersed in chloroform to a concentration of approximately 1 mg/mL. Three milliliters of this $PtNi_3$ nanopolyhedra solution was sonicated with 0.2 mL of oleylamine and diluted with 10 mL of hexadecane. This colloidal solution was sonicated for 30 min, followed by heating at 130 °C for 8 h in air to carry out the spontaneous oxidation and corrosion of $PtNi_3$ nanopolyhedra to Pt_3Ni nanoframes. Alternate combinations of temperature and timing can also be used during evolution, as reported previously. After evolution, the Pt_3Ni nanoframes were washed two times with hexane and ethanol and collected by centrifugation (8000 rpm). The washed nanoframes were re-dispersed in chloroform.

Preparation of Pt_3Ni/C Nanocatalyst and Testing. Pt_3Ni nanoframes dispersed in chloroform were added to carbon (Cabot, Vulcan XC-72) in a ratio which produced the desired loading of platinum on carbon. The actual loadings were determined by inductively coupled plasma mass spectrometry. The mixture was sonicated in chloroform for 30−45 min to complete the loading process. The catalyst was collected by centrifugation (10 000 rpm), washed once with hexanes, and recollected by centrifugation. The resulting catalyst powder was heated at 200 °C in air for at least 12 h in order to conduct simultaneous removal of organic surfactants and Pt-skin segregation. The catalyst was kept dry until preparation for electrochemical testing. Typically, the Pt_3Ni/C catalyst was dispersed in water with a concentration between 0.5 and 1 mg/mL. The catalyst ink was drop-cast onto a 6 mm glassy carbon disk in a volume of 10−20 μL and allowed to air-dry. The electrochemical measurements were conducted in a three-compartment electrochemical cell with a Pine rotating disk electrode (RDE) setup and an Autolab 302 potentiostat. A saturated Ag/AgCl electrode and a Pt wire were used as reference and counter electrodes, respectively, and 0.1 M $HClO_4$ was used as the electrolyte. In the following sections, all of the potentials are presented versus the reversible hydrogen electrode (RHE). The nanoframe catalyst was typically held at 0.05 V vs RHE between measurements, and the limits of the cyclic voltammetry (CV) were 0.05−1.0 V. Measurements with underpotentially deposited hydrogen were performed by saturating the electrolyte with argon gas before collecting the CV at a sweep rate of 50 mV/s. Electrooxidation of adsorbed CO, or CO-stripping measurements, were performed by purging CO through the electrolyte while holding the potential at 0.05 V. Argon was then purged to remove CO from the electrolyte and the CV was collected at a sweep rate of 50 mV/s. The ORR measurements were collected under O_2 purging conditions and at 20 mV/s with an RDE rotation rate of 1600 rpm. The current densities for ORR were corrected for ohmic *iR* drop.

X-ray Diffraction. Micro-X-ray diffraction (XRD) experiments were carried out at the Lawrence Berkeley National Laboratory Advanced Light Source (ALS) Beamline 10.3.2 with an energy of 17 keV corresponding to a wavelength of 0.729 Å. The detector used was a Bruker APEX II CCD detector and the sample-to-detector distance was calibrated with an α-Al_2O_3 standard. Data reduction was performed with FIT2D to obtain diffraction patterns in Q-space.

X-ray Absorption Measurements and Data Analysis. The Pt_3Ni/C catalyst ink was prepared at a concentration of 1 mg/mL in a solution of equal parts water and isopropanol and a concentration of 0.5% Nafion. A typical electrode for XAS was prepared with 20 μL of catalyst ink dropcast on a carbon paper substrate. A custom-made electrochemical cell was fabricated for *in situ* ORR measurements, in which the carbon paper acted as both the working electrode and X-ray transparent window (see images in Supporting Information). The electrochemical measurements were carried out in 0.1 M $HClO_4$ using a Ag/AgCl reference electrode and a platinum wire counter electrode. The electrolyte was continuously purged with high purity oxygen for ORR.

X-ray absorption near-edge structure (XANES) and extended X-ray absorption fine structure (EXAFS) data were collected at the ALS Beamline 10.3.2. The X-ray wavelength was monochromatized by a

DOI: 10.1021/jacs.5b09639
J. Am. Chem. Soc. 2015, 137, 15817−15824

Si(111) double-crystal, fixed exit monochromator. The intensity of the incident X-ray radiation, I_0, was monitored with a nitrogen filled ionization chamber. All data were collected in fluorescence mode with a 7-element Ge detector (Canberra). The data at the Ni K-edge and Pt L_3-edge were calibrated to a Ni foil and Pt foil, respectively. All spectra at a given edge were aligned according to a glitch in I_0 near each absorption edge.

XANES and EXAFS data reduction and EXAFS fitting was performed using the IFEFFIT based programs Athena and Artemis.[35] Edge step normalization for each spectra was performed by subtracting the pre-edge and post-edge backgrounds in Athena. For EXAFS background removal, a cubic spline was fit to the data and the *k*-space data were Fourier transformed resulting in an *R*-space spectrum which was fit in Artemis. EXAFS data were fit to the following EXAFS function:

$$\chi(k) = S_0^2 \sum_{i=1}^{\text{shells}} \frac{N_i}{kR_i^2} F_i(k)\, e^{-2k^2\sigma_i^2}\, e^{-2R_i/\lambda(k)} \sin[2kR_i - \varphi_i(k)]$$

The amplitude of the contribution from each coordination shell in the EXAFS function is summed to generate a fit to the data. S_0^2 represents an amplitude reduction factor which is typically assumed to be chemically transferable and is affected by shakeup effects at the absorbing atom.[36] It was estimated by performing a fit to EXAFS transmission measurements on Ni and Pt metal foils. Values for S_0^2 were determined to be 0.80 for Pt and 0.78 for Ni. N_i and R_i are the coordination number and half-path length between the central absorbing atom and a scattering atom, respectively. The mean-square disorder in the distance from the central absorbing atom to a given shell due to thermal fluctuation and structural disorder is represented by σ_i^2. These parameters are calculated by fitting the experimental data. The photoelectron mean free path is represented by λ. Lastly, $F_i(k)$ is the backscattering amplitude and $\varphi_i(k)$ is the phase factor for a given coordination shell. These parameters are calculated through *ab initio* methods using FEFF6 as embedded in Artemis and Atoms.

RESULTS AND DISCUSSION

Evaluation of Pt-Skin Formation on Pt_3Ni/C catalyst. $PtNi_3$ rhombic dodecahedra were synthesized as previously reported.[25] The ideal synthetic result of monodisperse, rhombic dodecahedral nanoparticles with sufficient segregation of the Pt-rich phase to the edges is highly sensitive to certain conditions, including precise temperature of the solvent and incorporation of trace oxygen and water during the hot injection process. In contrast, the evolution to nanoframe is straightforward and can be carried out at a variety of temperatures for different lengths of time. It has been found that the extent of evolution from a dodecahedron to a hollow nanoframe is not critical to the overall performance of the nanocatalyst as excess nickel will always be washed away during electrochemical testing such that the final nanoframe catalyst has the composition Pt_3Ni after electrochemical testing. After the evolution process, the nanoframes were incorporated into the high surface area carbon support and the dry catalyst powder was annealed at 200 °C in air in order to remove the ligands and induce platinum surface segregation to form a Pt-skin structure (Figure S2).[37] Temperatures above approximately 250 °C can cause the nanoframes to sinter, so special care was taken that the temperature never exceeded this limit. After annealing, the Pt_3Ni/C nanocatalyst was mixed with water to form the catalyst ink, and the glassy carbon RDE electrodes were prepared.

The success of Pt-skin structure formation was estimated by electrooxidation of carbon monoxide and underpotentially deposited hydrogen. It has been shown that both H_{upd} and CO_{ad} can be good estimates of platinum surface area by assuming ~210 $\mu C/cm^2$ transferred during a one-electron process (H_{upd}) or ~420 $\mu C/cm^2$ for a two-electron process (CO_{ad}).[17,38] On a Pt-skin surface, the binding to H_{upd} species is weakened such that the surface coverage of adsorbed hydrogen decreases by a factor of approximately one-third. Since CO_{ad} is a much more strongly bound species, its surface coverage on platinum does not change appreciably, making the surface area estimated by CO-stripping the more accurate method for a Pt-skin surface.

As mentioned above, characteristic ratios of CO_{ad}:H_{upd} electrochemical surface area have been measured for the Pt-skin surface of single-crystalline $Pt_3Ni(111)$ and the pure Pt(111) surface, yielding values of 1.5 and 1.0, respectively.[12] Pt-skin formation on PtNi nanoparticles has been previously demonstrated by first acid washing to prepare an atomically thin and rough Pt surface, followed by annealing to form a multilayered Pt-skin surface.[17] Similarly, in the case of Pt_3Ni nanoframes, successful platinum nanosegregation to form a Pt-skin is indicated by a CO_{ad}:H_{upd} ratio of 1.5. In contrast, nanoframe samples which demonstrate lower activity typically exhibit a CO_{ad}:H_{upd} ratio close to 1.0. The nanoframes are always synthesized in the same system, but the catalytic activity of the resulting structure does not always reach the values previously reported for a nanoframe with CO_{ad}:H_{upd} ratio of 1.5.[25] The H_{upd} and CO_{ad} cyclic voltammograms for Pt_3Ni nanoframes with evidently different types of surface conditions, demonstrated by CO_{ad}:H_{upd} ratios calculated as 1.0 and 1.5, are shown in Figure 1a-b. These electrochemically determined

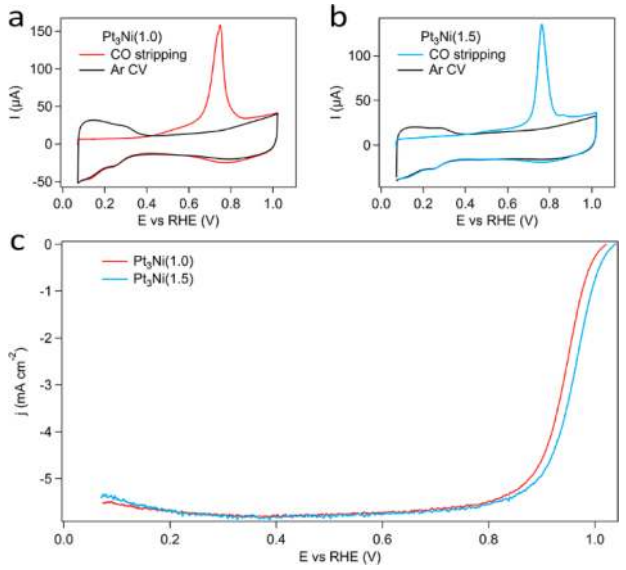

Figure 1. (a,b) Cyclic voltammograms in Ar and electrooxidation of adsorbed CO used to estimate ECSA for different Pt_3Ni nanoframes. Nanoframes with CO_{ad}:H_{upd} ratio equal to 1.0 and 1.5 are referred to as $Pt_3Ni(1.0)$ and $Pt_3Ni(1.5)$ respectively. (c) ORR curves normalized to projected area of the electrode illustrate differences in activity between $Pt_3Ni(1.0)$ and $Pt_3Ni(1.5)$.

ratios are indicators of the different binding strength between the surface and adsorbates. Figure 1c shows that the CO_{ad}:H_{upd} ratio greatly affects the activity for ORR, with $Pt_3Ni(1.0)$ having a specific activity of 0.75 mA/cm^2 and $Pt_3Ni(1.5)$ having activity of 1.46 mA/cm^2 (at 0.95 V vs RHE). The reported specific activity is based on the CO-stripping measurement. In order to depict the differences in atomic structure of Pt_3Ni

DOI: 10.1021/jacs.5b09639
J. Am. Chem. Soc. 2015, 137, 15817−15824

nanoframes with ECSA ratios of 1.5 and 1.0, we employed *ex situ* and *in situ* XAS.

***Ex Situ* XANES and EXAFS Analysis of As-Prepared Pt_3Ni/C.** X-ray absorption spectroscopy at the Ni K-edge and Pt L_3-edge was carried out at ALS Beamline 10.3.2. The XANES region can provide information on oxidation state based on the edge position and white line intensity. The edge position is typically defined as the peak in the first derivative of the absorption spectrum and becomes more positive for more oxidized species due to differences in the final state energy after photo-ejection of a core electron and generation of the core hole.[39−41] The white line intensity is the main peak in the absorption spectrum just after the edge. It increases in intensity for an oxidized species because of the larger probability for an X-ray absorption event to occur due to the increased availability of electronic states.[42,43] As can be seen from Figure 2a, after

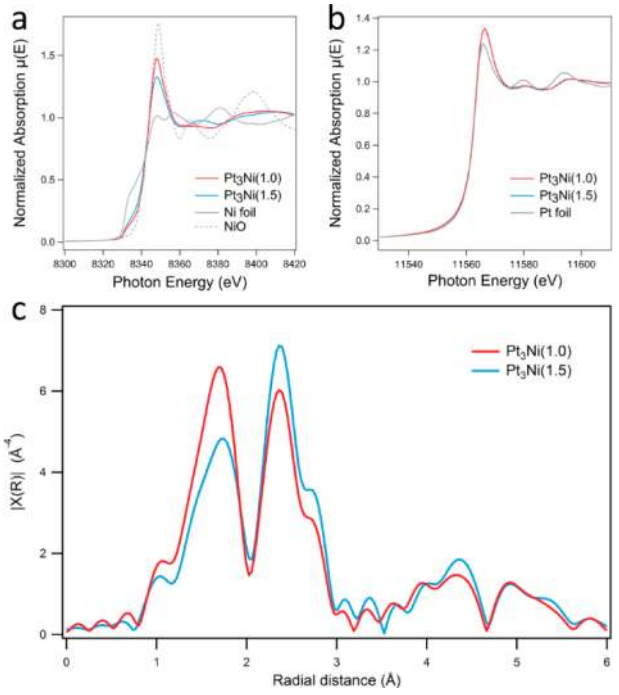

Figure 2. X-ray absorption spectroscopy of Pt_3Ni/C catalysts before electrochemistry: (a) Ni K-edge XANES compared to Ni foil and NiO powder standards. (b) Pt L_3-edge XANES compared to Pt foil standard. (c) Ni K-edge EXAFS spectra.

annealing of the catalyst in air, the nickel is in a more oxidized state relative to nickel metal. The extent of nickel oxidation is indicated by a positive increase of the absorption edge position in the range of 8331−8337 eV and an increase in the white line intensity at ∼8348 eV. The level of nickel oxidation for both the $Pt_3Ni(1.0)$ and $Pt_3Ni(1.5)$ samples is between Ni^0 and Ni^{2+} when compared to XANES spectra of Ni foil and NiO standards. This demonstrates the co-existence of two nickel species: one in a surface nickel oxide that remains after the evolution and annealing processes and one in the Pt_3Ni alloy. According to previous literature on surface segregation in PtNi octahedra, nickel will segregate to the surface as an oxidized species after annealing at 200 °C in 1 bar O_2.[44] In the Pt_3Ni nanoframe system, nickel at or near the surface of the nanoframe after evolution from solid particle to nanoframe will be oxidized during annealing at 200 °C in air, while nickel in the bulk alloy will remain alloyed. The result is small oxidized clusters of nickel on the surface of the nanoframe which can be removed during electrochemical treatment. The nickel in $Pt_3Ni(1.0)$ is more oxidized than in $Pt_3Ni(1.5)$, indicating that a larger quantity of surface NiO clusters remain in the $Pt_3Ni(1.0)$ nanoframe after evolution and annealing. This confirms that after the evolution process, there was more nickel present at the surface of the nanoframe in $Pt_3Ni(1.0)$ relative to $Pt_3Ni(1.5)$. It is important to note that synchrotron-based XRD, which takes advantage of high photon flux and high energy, short wavelength X-rays, could not detect crystalline nickel oxide in the Pt_3Ni nanoframes (Figure S3), indicating that the oxidized nickel species exist as very small domains of low crystallinity. The Pt L_3-edge XANES (Figure 2b) indicates that the platinum in $Pt_3Ni(1.0)$ and $Pt_3Ni(1.5)$ has a similar oxidation state which is slightly more oxidized than bulk Pt in a Pt foil standard.

While XANES provides information on oxidation state, EXAFS is utilized to acquire structural parameters such as coordination numbers, bond lengths, and the extent of alloying in a bimetallic nanoparticle.[45] In the post-edge region, the X-ray photon absorption creates a photoelectron wave which propagates outward from the absorbing atom. This wave can be scattered off of neighboring atoms, causing interference between the outward propagating wave and the backscattered wave. This interference can be constructive or destructive and causes the fine structure in an X-ray absorption spectrum by modulating the absorption coefficient. Because the scattering of the photoelectron wave is dependent on the distance between atoms and the identity of those atoms, coordination information can be extracted from EXAFS data. EXAFS data at the Ni K-edge and Pt L_3-edge were co-refined in order to analyze the atomic structure of $Pt_3Ni(1.0)$ and $Pt_3Ni(1.5)$. After annealing of the catalyst and before electrochemistry, further proof of the surface nickel oxide can be seen in the Ni K-edge R-space EXAFS spectra in which there is a first coordination shell at ∼1.7 Å indicative of Ni−O scattering (Figure 2c). The EXAFS spectra in Figure S4 were fit to a combination of a disordered face-centered cubic platinum nickel alloy model and a nickel oxide model. Due to the small nature of the nickel oxide species, only a first-shell Ni−O scattering path was included in modeling the nickel oxide species because any further Ni−Ni or Ni−O scattering paths were not significant. The nickel−oxygen coordination number derived from the fit, shown in Table S1, supports the conclusion that the $Pt_3Ni(1.0)$ nanoframe has a higher concentration of surface NiO clusters than $Pt_3Ni(1.5)$. The fit also shows that platinum is already segregated to the surface in the $Pt_3Ni(1.5)$ evidenced by the lower total coordination number for platinum than nickel. Surface atoms have fewer neighbors, reducing their average coordination number measured by EXAFS modeling.[46] In $Pt_3Ni(1.0)$, nickel is still slightly enriched at the surface of the frames, supporting the observation of greater nickel oxide formation on these nanoframes. In summary, after annealing treatment, both nanoframe samples exhibit formation of oxidized nickel clusters at their surfaces. This allows for Pt-enrichment beneath the clusters, as demonstrated in the as-prepared EXAFS of $Pt_3Ni(1.5)$.

***In Situ* XANES and EXAFS Analysis of Pt_3Ni/C for ORR.** Before probing the catalyst *in situ*, the electrode was electrochemically annealed with a cycling process which is standard procedure in an RDE set up to allow the catalyst to reach a steady-state composition and surface structure. The

DOI: 10.1021/jacs.5b09639
J. Am. Chem. Soc. 2015, 137, 15817−15824

catalyst film on carbon paper for XAS was prepared with similar thickness to an RDE catalyst film so that all metal sites were considered electrochemically accessible. After cycling of the electrode, XANES spectra were collected at the Ni K-edge and Pt L_3-edge at 0.9 V vs RHE under oxygen to replicate ORR conditions. First, it is evident in Figure 3a through the decrease

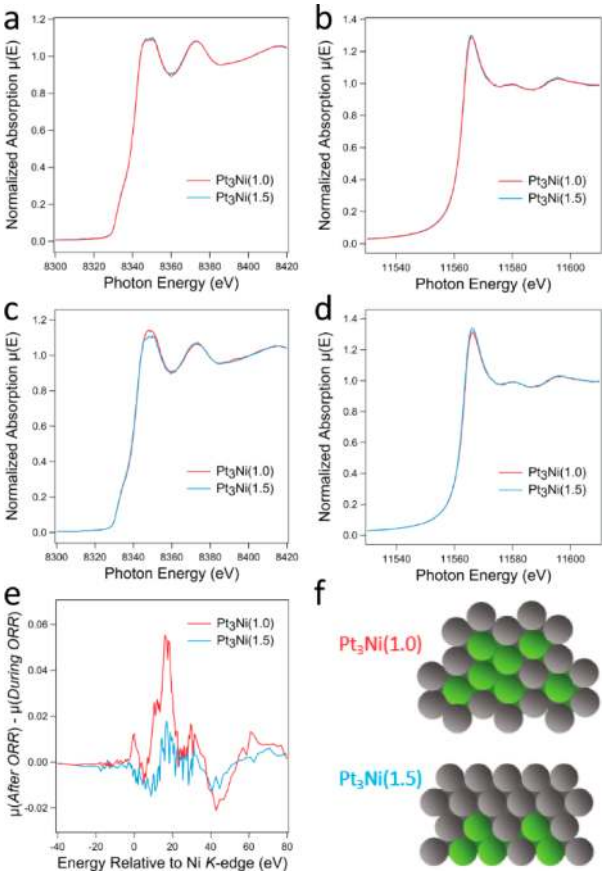

Figure 3. XANES of Pt_3Ni/C catalysts *in situ* and after electrochemistry: (a) Ni K-edge at 0.9 V. (b) Pt L_3-edge at 0.9 V. (c) Ni K-edge after *in situ*. (d) Pt L_3-edge after *in situ*. (e) Ni K-edge *in situ* XANES subtracted from after *in situ* XANES. (f) Model surfaces of $Pt_3Ni(1.0)$ and $Pt_3Ni(1.5)$, where gray atoms are Pt and green atoms are Ni.

in white line intensity that the surface NiO has dissolved in the acidic electrolyte after potential cycling, giving the Ni XANES spectrum more metallic character. It was also found that at both metal edges, the XANES spectra were identical, and therefore, the oxidation states of both metals in both samples were deemed identical (Figure 3a,b). The near-edge region of X-ray absorption probes electronic transitions from a core level into local, unoccupied states just above the Fermi level energy. During *in situ* ORR, the Fermi levels of the Pt_3Ni metallic samples are controlled by the potentiostat at an identical potential relative to a reference electrode potential.[47] Therefore, the probability of an X-ray absorption-induced transition into the unoccupied states is similar for these samples while under potential control, and their XANES spectra are identical. However, as can be seen from Figure 3c,d, after the electrode is removed from the electrolyte, rinsed, and dried, the XANES spectra are no longer identical between $Pt_3Ni(1.0)$ and $Pt_3Ni(1.5)$. The Ni in $Pt_3Ni(1.0)$ is more oxidized while the Pt is more reduced, indicating increased donation of electron density from Ni to Pt in $Pt_3Ni(1.0)$.[48] The increased alloying in $Pt_3Ni(1.0)$ will be further supported by the EXAFS analysis discussed below. Figure 3e shows a XANES difference spectrum at the Ni K-edge for $Pt_3Ni(1.0)$ and $Pt_3Ni(1.5)$ samples where the normalized absorption *in situ* is subtracted from the normalized absorption after ORR. After the catalyst is rinsed and dried under nitrogen, the nickel in $Pt_3Ni(1.0)$ is more easily oxidized as indicated by the more intense peak at the white line position, approximately 16−17 eV after the edge. The platinum shell is not protecting the nickel as thoroughly in $Pt_3Ni(1.0)$, suggesting the surface has more low coordination sites and a thinner platinum shell, as illustrated in Figure 3f. These conclusions will be further substantiated by EXAFS data.

In situ EXAFS analysis yields a clear picture of the differences in atomic distribution and structuring in $Pt_3Ni(1.0)$ and $Pt_3Ni(1.5)$. As stated earlier, the working electrode was cycled in order to condition the catalyst and then held at 0.9 V vs RHE for *in situ* ORR. The Fourier transformed EXAFS spectra are shown in Figure 4. EXAFS data for Pt and Ni foils were taken in order to execute a fit on the bulk sample and determine the S_0^2 parameter, which was then used during fitting of the nanoframe EXAFS spectra. A fit to the first shell was performed using identical bounds in R-space for $Pt_3Ni(1.0)$ and $Pt_3Ni(1.5)$. A disordered face-centered cubic Pt_3Ni model was created in order to generate the first shell homo- and heterometallic scattering paths. Coordination numbers, path lengths, and mean-square disorder parameters were allowed to float with the restraints that $R_{PtNi} = R_{NiPt}$ and $\sigma^2_{PtNi} = \sigma^2_{NiPt}$. The identical fitting procedure was used for all first shell fits, and the fitted parameters are shown in Table 1. Extended shell fitting was unsuccessful due to the disordered nature of the alloy and the small dimension of a single nanoframe edge, which is approximately 2 nm in width, leading to a reduced amplitude of the outer shells. The initial observation in the first shell fit is that the total coordination numbers N_{Pt} and N_{Ni} are similar for both samples, with N_{Pt} significantly smaller than N_{Ni}. As mentioned previously, this indicates that Pt atoms have segregated to the surface to form some variation of the desired Pt-skin structure because of the lower coordination number of surface atoms. It can also be seen that the heterometallic coordination of nickel to platinum is decreased in $Pt_3Ni(1.5)$, and correspondingly the homometallic coordination is increased. This depicts the nanoframe of $Pt_3Ni(1.5)$ as one with more segregation of Pt from Ni, which is also indicated by the smaller extent of alloying parameters for platinum, J_{Pt}, calculated for $Pt_3Ni(1.5)$ versus $Pt_3Ni(1.0)$. The extent of alloying parameters are calculated using the coordination numbers determined from EXAFS according to the method developed by Hwang et al.[49]

The composition of the nanoframe can be determined by[50]

$$\frac{X_{Pt}}{X_{Ni}} = \frac{N_{NiPt}}{N_{PtNi}}$$

The sensitivity of the EXAFS measurement allows for estimation of slight variations in composition of $Pt_3Ni(1.0)$ and $Pt_3Ni(1.5)$ from the nominal value of the thermodynamically favorable, ordered Pt_3Ni state. It was determined from *in situ* EXAFS measurements that $Pt_3Ni(1.0)$ was 28% nickel while $Pt_3Ni(1.5)$ was 22% nickel. It is expected that the composition will not be exactly that of Pt_3Ni because the final composition of the nanoframe must be influenced by the amount of platinum segregation to the edge of the initial dodecahedra that

DOI: 10.1021/jacs.5b09639
J. Am. Chem. Soc. 2015, 137, 15817−15824

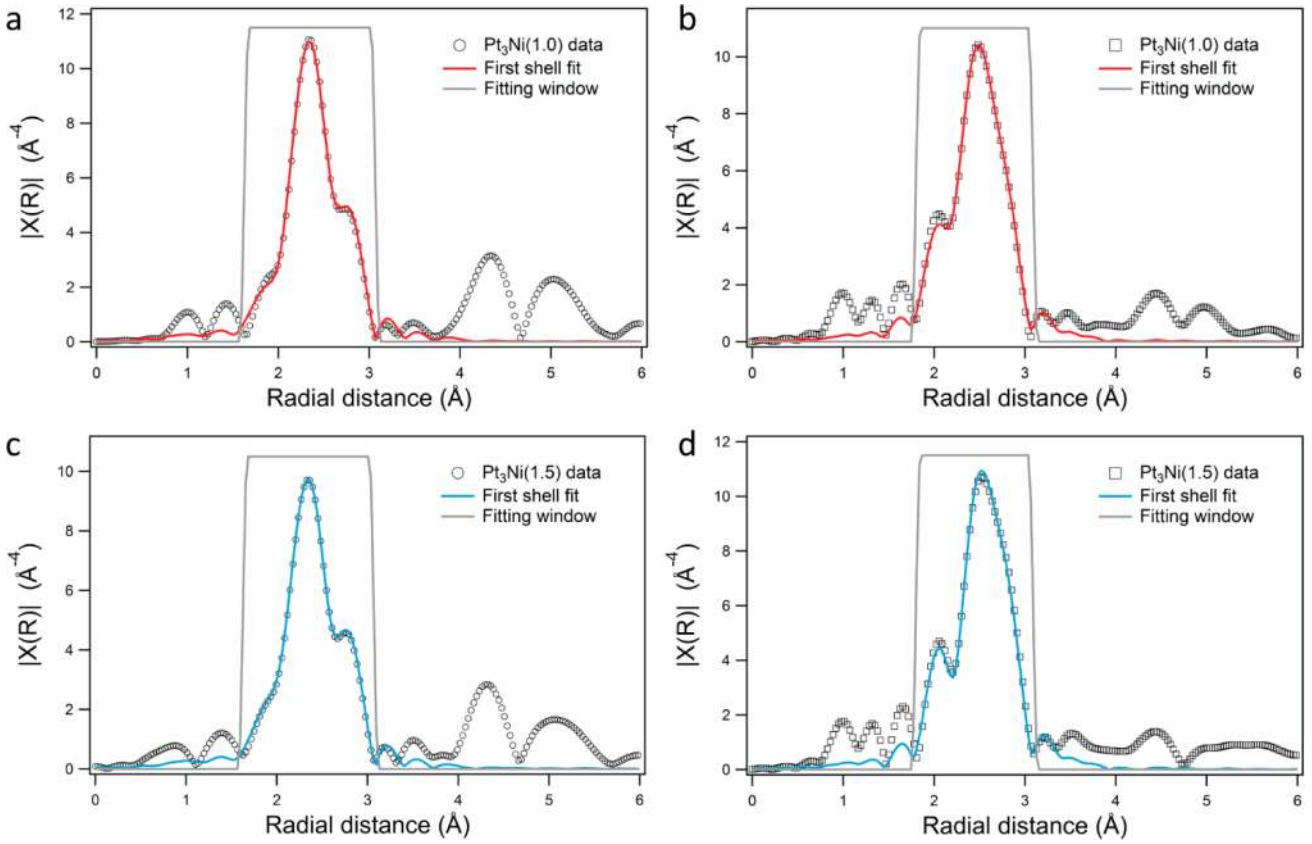

Figure 4. *In situ* experimental EXAFS spectra and fits to the first coordination shell: (a) Ni K-edge EXAFS of $Pt_3Ni(1.0)$. (b) Pt L_3-edge EXAFS of $Pt_3Ni(1.0)$. (c) Ni K-edge EXAFS of $Pt_3Ni(1.5)$. (d) Pt L_3-edge EXAFS of $Pt_3Ni(1.5)$. For Pt EXAFS, Δk = 2.0−13.5 Å^{-1} and ΔR = 1.8−3.1 Å. For Ni EXAFS, Δk = 2.0−12.0 Å^{-1} and ΔR = 1.6−3.1 Å.

Table 1. Fitting Parameters for First-Shell Fits of *in Situ* EXAFS Spectra[a]

	N_{PtNi}	N_{NiPt}	N_{PtPt}	N_{NiNi}	N_{Pt}	N_{Ni}	R_{PtNi}	R_{PtPt}	R_{NiNi}	J_{Pt} (%)	J_{Ni} (%)
$Pt_3Ni(1.0)$	2.5 (0.5)	6.4 (0.9)	6.0 (0.7)	3.9 (0.7)	8.5 (1.2)	10.3 (1.6)	2.657 (0.006)	2.716 (0.004)	2.648 (0.007)	117	83
$Pt_3Ni(1.5)$	1.8 (0.5)	6.4 (1.1)	6.9 (0.8)	4.0 (1.0)	8.7 (1.3)	10.4 (2.1)	2.666 (0.007)	2.728 (0.004)	2.655 (0.010)	82	82

[a]Values in parentheses are error bars determined from IFEFFIT.

were synthesized. The spontaneous corrosion to the nanoframe is a kinetically controlled process that does not access the thermodynamically stable, ordered Pt_3Ni phase, given the disordered structure of the initial bimetallic particle. A nickel-rich nanoframe in the case of $Pt_3Ni(1.0)$ is further supported by the shorter bond lengths which were measured by EXAFS modeling. Due to a slightly larger incorporation of the smaller element, nickel, the bond lengths in $Pt_3Ni(1.0)$ are shorter.

The *ex situ* post-ORR EXAFS data were collected after the catalyst film was rinsed with ultrapure water and dried under N_2 (Figure S5). We emphasize that the EXAFS analysis showed the same trends in coordination numbers, bond lengths, extent of alloying, and alloy composition between $Pt_3Ni(1.0)$ and $Pt_3Ni(1.5)$ after ORR as the *in situ* measurement, indicating good reproducibility of the technique (Table S2).

Model of *ex Situ* and *in Situ* Pt_3Ni/C Surfaces. The information gathered from *ex situ* and *in situ* XANES and EXAFS measurements on Pt_3Ni nanoframe ORR catalysts provides an understanding of the structure of the more active $Pt_3Ni(1.5)$ catalysts. After evolution from nanopolyhedra to nanoframes, the nanoframes have platinum and nickel present at their surfaces, with $Pt_3Ni(1.5)$ slightly enriched in platinum at its surface. The annealing process in air atmosphere induces the formation of surface nickel oxide clusters while allowing for Pt enrichment beneath the nickel oxide clusters in $Pt_3Ni(1.5)$. $Pt_3Ni(1.5)$ has fewer nickel oxide clusters due to a larger presence of platinum on the surface of the nanoframe. The larger concentration of platinum on the surface of the $Pt_3Ni(1.5)$ nanoframe after the evolution process is attributed to better segregation of platinum to the edges of the initially synthesized rhombic dodecahedron. Anisotropic elemental distribution and phase segregation within a bimetallic nanocrystal have been previously observed in Pt−Ni octahedra as well,[51] and play a key role in the successful spontaneous corrosion of a solid rhombic dodecahedron into a $Pt_3Ni(1.5)$ nanoframe. The complete formation of the Pt-rich framework at the edges of the initial solid polyhedron makes it easier to extract nickel from the interior of the polyhedron during the spontaneous corrosion to a hollow nanoframe. Figure 5a,b illustrates the differences between the surface and alloying conditions of a cross-section of an edge of the $Pt_3Ni(1.0)$ and $Pt_3Ni(1.5)$ nanoframe before electrochemistry. The nickel atoms at the surface are representative of nickel oxide clusters which form after annealing in air. Once the nanoframe samples

DOI: 10.1021/jacs.5b09639
J. Am. Chem. Soc. 2015, 137, 15817−15824

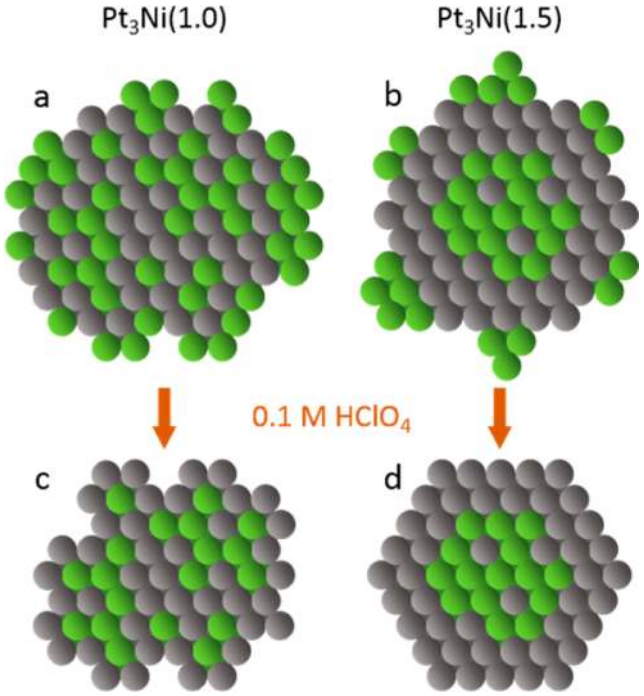

Figure 5. Models of the atomic level structure of the edge of the $Pt_3Ni(1.0)$ and $Pt_3Ni(1.5)$ nanoframes (shown in cross-section) before electrochemistry (a,b) and *in situ* during ORR catalysis (c,d). Gray atoms are Pt and green atoms are Ni.

are immersed in the electrolyte, 0.1 M $HClO_4$, and electrochemically annealed, the nickel oxide is dissolved from the surface, leaving pure platinum. *In situ* EXAFS analysis reveals more significant segregation of Pt from Ni in $Pt_3Ni(1.5)$ and slightly nickel-rich composition of $Pt_3Ni(1.0)$. The alloying data extracted from the EXAFS analysis of $Pt_3Ni(1.0)$ and $Pt_3Ni(1.5)$ once removed from electrolyte, rinsed, and dried, reflected identical differences as during *in situ* measurements. However, it was observed that nickel in the $Pt_3Ni(1.0)$ nanoframe was slightly more oxidized compared to that in the $Pt_3Ni(1.5)$ after exposure to air, which is further evidence that nickel is present closer to the surface, covered by a thinner, lower-coordinated platinum shell. The conclusions made from this analysis before, during, and after ORR electrochemical measurements lead to the model shown in Figure 5c,d for the *in situ* atomic structuring of the edge of a nanoframe. The ideal nanoframe catalyst represented by $Pt_3Ni(1.5)$ forms a more uniform Pt-skin due to its increased segregation of platinum from nickel and slightly platinum-rich composition. The ability to form the ideal Pt-skin on the nanoframe is primarily predetermined by the initial synthesis of the rhombic dodecahedra and the amount of platinum segregation to the edges which is achieved. The extent of evolution toward the nanoframe, accelerated by solution-phase heating in the presence of oxygen, and the annealing step, are less critical to the formation of the ideal surface condition. If the segregation of platinum to the edges of the rhombic dodecahedron is not sufficient, the final nanoframe is likely to be enriched in nickel and have excessive nickel present at the surface of the nanoframe during annealing, preventing successful Pt-skin formation and causing a rough platinum surface to be exposed during electrochemistry. As has been observed on PtNi nanoparticles, the rough platinum surface exhibits a CO_{ad}:H_{upd} ratio of 1.0.[17] This decreased ratio compared to the $Pt_3Ni(1.5)$ is driven by adsorbates being more strongly bound due to the higher concentration of low coordination surface sites on the rougher platinum surface of the $Pt_3Ni(1.0)$. If the rhombic dodecahedron is synthesized with the desirable segregation of platinum to its edges, the nickel can be more thoroughly removed from the interior of the nanoframe and the nanoframe will form the desired Pt-skin during annealing. This ideal surface segregation of platinum changes the surface *d*-band electronic structure such that adsorbates are bound more weakly, simultaneously leading to the CO_{ad}:H_{upd} ratio of 1.5 and dramatically increased activity for the ORR.

CONCLUDING REMARKS

In summary, surface-sensitive electrochemical techniques and *ex situ* and *in situ* XAS were used to identify differences in atomic-level structure of Pt_3Ni nanoframe catalysts which led to differences in their ORR activity. Electrochemical surface area estimated from voltammograms of adsorbed H_{upd} and CO_{ad} were used to identify nanoframes with CO_{ad}:H_{upd} surface area ratios of 1.0 and 1.5. The ratio of 1.0 indicates the surface of the nanoframe that correlates with lesser activity for the ORR. In addition, the as-prepared $Pt_3Ni(1.0)$ demonstrated more abundant surface nickel oxide formation as compared to $Pt_3Ni(1.5)$. This nickel oxide was dissolved from the surface via electrochemical cycling in the acidic electrolyte, leaving behind a platinum surface. *In situ* EXAFS demonstrated that $Pt_3Ni(1.0)$ had a larger extent of alloying while $Pt_3Ni(1.5)$ had more significant segregation of Pt to the surface of the nanoframe. It was concluded that $Pt_3Ni(1.0)$ has a thinner, rougher Pt surface caused by insufficient segregation of Pt to the surface. $Pt_3Ni(1.5)$ exhibits extremely high ORR activity due to its significant segregation of Pt from Ni, allowing for better formation of a Pt-skin. The activity of a given nanoframe sample was resolved to be primarily pre-determined by the level of platinum enrichment at the edges of the initial rhombic dodecahedron.

ASSOCIATED CONTENT

Supporting Information

The Supporting Information is available free of charge on the ACS Publications website at DOI: 10.1021/jacs.5b09639.

Figures S1−S7 and Tables S1 and S2, showing images of *in situ* XAS cell, TEM images of catalysts, XRD, and EXAFS fits for as-prepared and after-electrochemistry conditions (PDF)

AUTHOR INFORMATION

Corresponding Author

*p_yang@berkeley.edu

Present Address

[∇]C.C.: Department of Chemistry, Tsinghua University, Beijing 100084, P. R. China

Notes

The authors declare no competing financial interest.

ACKNOWLEDGMENTS

The research conducted at Lawrence Berkeley National Laboratory and Argonne National Laboratory was supported by the U.S. Department of Energy, Office of Science, Office of Basic Energy Sciences, Materials Sciences and Engineering Division, under Contract No. DE-AC02-05CH11231 (surface)

DOI: 10.1021/jacs.5b09639
J. Am. Chem. Soc. 2015, 137, 15817−15824

and No. DE-AC02-06CH11357, respectively. The authors thank Matthew Marcus and Sirine Fakra for help with the XAS studies which were carried out at the Advanced Light Source BL 10.3.2. The Advanced Light Source is supported by the Director, Office of Science, Office of Basic Energy Sciences, U.S. Department of Energy, under Contract No. DE-AC02-05CH11231. J.R. gratefully acknowledges support from the National Science Foundation Graduate Research Fellowship Proposal (NSF GRFP) under Grant No. DGE-0802270 and the UC Berkeley Chancellor's Fellowship.

REFERENCES

(1) Lewis, N. S.; Nocera, D. G. *Proc. Natl. Acad. Sci. U. S. A.* **2006**, *103*, 15729.
(2) Dresselhaus, M.; Thomas, I. *Nature* **2001**, *414*, 332.
(3) Kim, D.; Sakimoto, K. K.; Hong, D.; Yang, P. *Angew. Chem., Int. Ed.* **2015**, *54*, 3259.
(4) Markovic, N. M.; Schmidt, T. J.; Stamenkovic, V.; Ross, P. N. *Fuel Cells* **2001**, *1*, 105.
(5) Zhang, J. L.; Vukmirovic, M. B.; Xu, Y.; Mavrikakis, M.; Adzic, R. R. *Angew. Chem., Int. Ed.* **2005**, *44*, 2132.
(6) Debe, M. K. *Nature* **2012**, *486*, 43.
(7) Gasteiger, H. A.; Marković, N. M. *Science* **2009**, *324*, 48.
(8) Stamenkovic, V. R.; Fowler, B.; Mun, B. S.; Wang, G. F.; Ross, P. N.; Lucas, C. A.; Markovic, N. M. *Science* **2007**, *315*, 493.
(9) Stamenkovic, V.; Mun, B. S.; Mayrhofer, K. J. J.; Ross, P. N.; Markovic, N. M.; Rossmeisl, J.; Greeley, J.; Norskov, J. K. *Angew. Chem., Int. Ed.* **2006**, *45*, 2897.
(10) Stamenkovic, V. R.; Mun, B. S.; Arenz, M.; Mayrhofer, K. J. J.; Lucas, C. A.; Wang, G. F.; Ross, P. N.; Markovic, N. M. *Nat. Mater.* **2007**, *6*, 241.
(11) Hammer, B.; Norskov, J. *Nature* **1995**, *376*, 238.
(12) van der Vliet, D. F.; Wang, C.; Li, D. G.; Paulikas, A. P.; Greeley, J.; Rankin, R. B.; Strmcnik, D.; Tripkovic, D.; Markovic, N. M.; Stamenkovic, V. R. *Angew. Chem., Int. Ed.* **2012**, *51*, 3139.
(13) Mayrhofer, K. J. J.; Strmcnik, D.; Blizanac, B. B.; Stamenkovic, V.; Arenz, M.; Markovic, N. M. *Electrochim. Acta* **2008**, *53*, 3181.
(14) Schmidt, T. J.; Gasteiger, H. A.; Staeb, G. D.; Urban, P. M.; Kolb, D. M.; Behm, R. J. *J. Electrochem. Soc.* **1998**, *145*, 2354.
(15) Zhang, J.; Yang, H. Z.; Fang, J. Y.; Zou, S. Z. *Nano Lett.* **2010**, *10*, 638.
(16) Wu, J.; Zhang, J.; Peng, Z.; Yang, S.; Wagner, F. T.; Yang, H. *J. Am. Chem. Soc.* **2010**, *132*, 4984.
(17) Wang, C.; Chi, M. F.; Li, D. G.; Strmcnik, D.; van der Vliet, D.; Wang, G. F.; Komanicky, V.; Chang, K. C.; Paulikas, A. P.; Tripkovic, D.; Pearson, J.; More, K. L.; Markovic, N. M.; Stamenkovic, V. R. *J. Am. Chem. Soc.* **2011**, *133*, 14396.
(18) Wu, J. B.; Gross, A.; Yang, H. *Nano Lett.* **2011**, *11*, 798.
(19) Cui, C.; Gan, L.; Li, H.; Yu, S.; Heggen, M.; Strasser, P. *Nano Lett.* **2012**, *12*, 5885.
(20) van der Vliet, D. F.; Wang, C.; Tripkovic, D.; Strmcnik, D.; Zhang, X. F.; Debe, M. K.; Atanasoski, R. T.; Markovic, N. M.; Stamenkovic, V. R. *Nat. Mater.* **2012**, *11*, 1051.
(21) Carpenter, M. K.; Moylan, T. E.; Kukreja, R. S.; Atwan, M. H.; Tessema, M. M. *J. Am. Chem. Soc.* **2012**, *134*, 8535.
(22) Cui, C.; Gan, L.; Heggen, M.; Rudi, S.; Strasser, P. *Nat. Mater.* **2013**, *12*, 765.
(23) Choi, S. I.; Xie, S. F.; Shao, M. H.; Odell, J. H.; Lu, N.; Peng, H. C.; Protsailo, L.; Guerrero, S.; Park, J. H.; Xia, X. H.; Wang, J. G.; Kim, M. J.; Xia, Y. N. *Nano Lett.* **2013**, *13*, 3420.
(24) Huang, X.; Zhao, Z.; Cao, L.; Chen, Y.; Zhu, E.; Lin, Z.; Li, M.; Yan, A.; Zettl, A.; Wang, Y. M.; Duan, X.; Mueller, T.; Huang, Y. *Science* **2015**, *348*, 1230.
(25) Chen, C.; Kang, Y.; Huo, Z.; Zhu, Z.; Huang, W.; Xin, H. L.; Snyder, J. D.; Li, D.; Herron, J. A.; Mavrikakis, M.; Chi, M.; More, K. L.; Li, Y.; Marković, N. M.; Somorjai, G. A.; Yang, P.; Stamenkovic, V. R. *Science* **2014**, *343*, 1339.
(26) Cremer, P. S.; Su, X.; Shen, Y. R.; Somorjai, G. A. *J. Am. Chem. Soc.* **1996**, *118*, 2942.
(27) Tao, F.; Grass, M. E.; Zhang, Y.; Butcher, D. R.; Renzas, J. R.; Liu, Z.; Chung, J. Y.; Mun, B. S.; Salmeron, M.; Somorjai, G. A. *Science* **2008**, *322*, 932.
(28) Mukerjee, S.; Srinivasan, S.; Soriaga, M. P.; McBreen, J. *J. Electrochem. Soc.* **1995**, *142*, 1409.
(29) Zheng, F.; Alayoglu, S.; Guo, J.; Pushkarev, V.; Li, Y.; Glans, P.-A.; Chen, J.-l.; Somorjai, G. *Nano Lett.* **2011**, *11*, 847.
(30) Jia, Q.; Caldwell, K.; Ramaker, D. E.; Ziegelbauer, J. M.; Liu, Z.; Yu, Z.; Trahan, M.; Mukerjee, S. *J. Phys. Chem. C* **2014**, *118*, 20496.
(31) Caldwell, K. M.; Ramaker, D. E.; Jia, Q.; Mukerjee, S.; Ziegelbauer, J. M.; Kukreja, R. S.; Kongkanand, A. *J. Phys. Chem. C* **2015**, *119*, 757.
(32) Jia, Q.; Liang, W.; Bates, M. K.; Mani, P.; Lee, W.; Mukerjee, S. *ACS Nano* **2015**, *9*, 387.
(33) Friebel, D.; Miller, D. J.; O'Grady, C. P.; Anniyev, T.; Bargar, J.; Bergmann, U.; Ogasawara, H.; Wikfeldt, K. T.; Pettersson, L. G. M.; Nilsson, A. *Phys. Chem. Chem. Phys.* **2011**, *13*, 262.
(34) Casalongue, H. S.; Kaya, S.; Viswanathan, V.; Miller, D. J.; Friebel, D.; Hansen, H. A.; Nørskov, J. K.; Nilsson, A.; Ogasawara, H. *Nat. Commun.* **2013**, *4*, 2817.
(35) Ravel, B.; Newville, M. *J. Synchrotron Radiat.* **2005**, *12*, 537.
(36) Koningsberger, D. C.; Mojet, B. L.; van Dorssen, G. E.; Ramaker, D. E. *Top. Catal.* **2000**, *10*, 143.
(37) Li, D. G.; Wang, C.; Tripkovic, D.; Sun, S. H.; Markovic, N. M.; Stamenkovic, V. R. *ACS Catal.* **2012**, *2*, 1358.
(38) Trasatti, S.; Petrii, O. *Pure Appl. Chem.* **1991**, *63*, 711.
(39) Fernández-García, M. *Catal. Rev.: Sci. Eng.* **2002**, *44*, 59.
(40) Pandya, K.; Hoffman, R.; McBreen, J.; O'Grady, W. *J. Electrochem. Soc.* **1990**, *137*, 383.
(41) De Groot, F. *Chem. Rev.* **2001**, *101*, 1779.
(42) Brown, M.; Peierls, R.; Stern, E. *Phys. Rev. B* **1977**, *15*, 738.
(43) Mansour, A. N.; Cook, J. W.; Sayers, D. E. *J. Phys. Chem.* **1984**, *88*, 2330.
(44) Ahmadi, M.; Behafarid, F.; Cui, C.; Strasser, P.; Roldan Cuenya, B. *ACS Nano* **2013**, *7*, 9195.
(45) Frenkel, A. I. *Chem. Soc. Rev.* **2012**, *41*, 8163.
(46) Frenkel, A. I. *J. Synchrotron Radiat.* **1999**, *6*, 293.
(47) Bard, A. J.; Faulkner, L. R. *Electrochemical methods: fundamentals and applications*; Wiley: New York, 1980; Vol. 2.
(48) Alayoglu, S.; Zavalij, P.; Eichhorn, B.; Wang, Q.; Frenkel, A. I.; Chupas, P. *ACS Nano* **2009**, *3*, 3127.
(49) Hwang, B.-J.; Sarma, L. S.; Chen, J.-M.; Chen, C.-H.; Shih, S.-C.; Wang, G.-R.; Liu, D.-G.; Lee, J.-F.; Tang, M.-T. *J. Am. Chem. Soc.* **2005**, *127*, 11140.
(50) Nashner, M. S.; Frenkel, A. I.; Somerville, D.; Hills, C. W.; Shapley, J. R.; Nuzzo, R. G. *J. Am. Chem. Soc.* **1998**, *120*, 8093.
(51) Gan, L.; Cui, C.; Heggen, M.; Dionigi, F.; Rudi, S.; Strasser, P. *Science* **2014**, *346*, 1502.

DOI: 10.1021/jacs.5b09639
J. Am. Chem. Soc. 2015, 137, 15817−15824